Colloid Polym Sci (2004) 282: 810–824
DOI 10.1007/s00396-004-1128-x

ORIGINAL CONTRIBUTION

Rouja Ivanova
Rosina Staneva
Steffen Geppert
Barbara Heck
Bernd Walter
Wolfram Gronski
Bernd Stühn

Interplay between domain microstructure and nematic order in liquid crystalline/isotropic block copolymers

Received: 26 January 2004
Accepted: 2 April 2004
Published online: 4 May 2004

This paper is dedicated to Prof. Fischer on the occasion of his 75th birthday.

R. Ivanova · R. Staneva
B. Walter · B. Stühn (✉)
Technical Physics II/Polymer Physics,
Ilmenau Technical University,
PF 100565, 98684 Ilmenau, Germany
E-mail:
stuehn@fkp.physik.tu-darmstadt.de

S. Geppert · B. Heck · W. Gronski
Institute for Macromolecular Chemistry,
Freiburg University, 79104 Freiburg,
Germany

Present address: B. Stühn
Experimental Condensed Matter Physics,
Institute of Solid State Physics,
Technical University of Darmstadt,
64289 Darmstadt, Germany

Abstract The domain microstructure and the nematic LC mesophase in a series of side-chain liquid crystalline/isotropic (LC/I) diblock copolymers with systematically varied block volume fractions were studied in a broad temperature range (25–170 °C) by DSC, polarized microscopy, and wide and small angle X-ray scattering. At all temperatures the block copolymers are microphase separated. The PSLC block copolymers exhibit order at two length-scales: on one hand, a nematic LC mesophase with characteristic length-scale of 0.43 nm (intermesogen distance); on the other hand, lamellar, hexagonal or cubic domain microstructures with characteristic length-scales of 27–44 nm (lattice parameter). The LC block was either located in the matrix or confined inside the microdomains. The thermotropic behavior is characterized by the sequence g/~35 °C/n/~115 °C/i and is not affected by the domain microstructure and/or dimensions. Analysis of the lamellar dimensions showed that the LC chain is stretched. With increasing temperature, a thermal expansion of both blocks takes place followed by a retraction of the LC chain above T_{NI}. The phase diagram is asymmetric and does not alter above T_{NI}. No order-to-order transitions triggered by the nematic-isotropic transition are observed. It was shown that domain microstructures of low interfacial curvature (lamellar and hexagonal) are energetically favored over the geometrically expected ones of high interfacial curvature (micellar cubic) due to the presence of nematic LC mesophase in the matrix or in the microdomains. By comparison to theory a Kuhn segment length of the LC block $b_{LC} = 0.86$ nm was derived from the location of the lamellar/hexagonal phase boundaries.

Keywords Thermotropic liquid crystalline behavior · Liquid crystalline block copolymers · Phase diagram · X-ray scattering

Introduction

This article deals with the study of ordering phenomena in a special class of block copolymers. The question of structure formation in polymers and the use of scattering methods in their investigation has been one of the many and very successful topics in the scientific career of Prof. E. W. Fischer. His comprehensive knowledge of polymer physics and his rigor in all scientific discussions has inspired and driven his coworkers and students and we (in particular B. S.) are very grateful for this experience.

The variety of lyotropic liquid crystalline (LC) microstructures attained by microphase-separated block copolymers are of practical interest and have been long

studied; e.g., [1, 2, 3, 4]. Depending on the application demands, different systems can be advantageous. Two-, three- or more component block copolymer-solvent systems offer a real diversity of microstructures and options for their modification, such as solvent-induced microphase separation, reversible gel-solution transition, etc. [5, 6, 7]. Such systems are readily used in the pharmaceutical industry for example. However, the presence of solvent(s) is often not desirable, while the demand for new easily attained structures with special functionalities remains. For example, the one-component block copolymer systems (dry polymer melts) are preferred in technological applications. In order to obtain structural variety in this case, one has to synthesize a large number of new block copolymers, which is not always straightforward. Such systems, however, offer possibilities for combination of anisotropic optical, electrical or mechanical properties with good thermal and physical resistance and durability [8, 9, 10].

In this context, the block copolymers containing one liquid crystalline and one isotropic block raise special practical as well as fundamental interest due to the combination of thermotropic LC behavior and mesomorphic microdomain morphologies. Essential questions to be investigated in such systems are, for example, microstructure formation, parameters governing the self-assembly and interaction between LC mesophase and domain structure.

The LC/I block copolymer systems are not so well-studied as LC homopolymers or I/I block copolymers (see reviews [11, 12]). Recently the first theoretical modeling of the thermotropic LC behavior and the microdomain morphology of side-chain LC/I block copolymers has been reported [13]. It shows that the conformational asymmetry, caused by the side-chain LC block, influences the microdomain shape and leads to an asymmetry of the phase diagram. The theoretical phase diagrams agree well with the available experimental ones [14, 15, 16, 17]. The theory predicts order-to-order transition from low-curvature microstructures to higher curvature microstructures at the isotropisation temperature of the LC block, that have indeed been experimentally registered [18, 19]. However, it cannot clarify the reverse type of order-to-order transitions observed by Hammond et al. [17]. Another open question is for example how the LC mesophase is affected by the microdomain confinement. Further experimental and theoretical investigations of various types of LC/I block copolymers can help to refine the model and to develop general theories of the phase behavior of such complex systems.

Here we present an investigation of the thermotropic LC behavior and the microdomain morphology of nematic side-chain LC/I diblock copolymers. Issues such as the formation of nematic LC mesophase and the formation of specific domain microstructures as well as their mutual influence are addressed.

Experimental section

Materials and chemical characterization A series of nine diblock copolymers consisting of a nematic side-chain liquid crystalline block (LC) and an isotropic block (PS), see Fig. 1, with well-defined chemical structure and systematically varied block volume fractions were synthesized using a modification of the three-step technique developed by Gronski et al. [20]. The synthesis and the chemical characterization of the precursor and the end-product polymers by SEC, FTIR or ^{1}H-NMR are reported in details in our previous work [21]. The end-product LC/I block copolymers are denoted as PSLC x/y where x is the volume percent of the PS block and y is the volume percent of the LC block (data are given in Table 1). Their molecular weight varies in the range 38,300–125,000 and has a very narrow distribution (M_w/M_n 1.03–1.10). The block weight fractions are calculated stoichiometrically provided that a 100% conversion of the precursor block copolymers into the end-products takes place [21]. The block volume fractions are calculated from the corresponding weight fractions using the density of the PS block (1.04 g/cm^3) and of the LC block (1.25 g/cm^3). Further, we have here performed an additional determination of the composition of the synthesized PSLC block copolymers using ^{1}H-NMR. The directly measured quantities, the number of the aromatic and the aliphatic protons per macromolecule, are converted into the corresponding degree of polymerization of the LC (N_{LC}) and the PS (N_{PS}) block. As Table 1 demonstrates, the experimentally obtained N_{LC}/N_{PS} values agree well with the calculated ones. The deviation was between 2% and 10% except for the block copolymer with the highest PS content. This result confirms that the synthesis has proceeded with practically 100% conversion and without side-reactions.

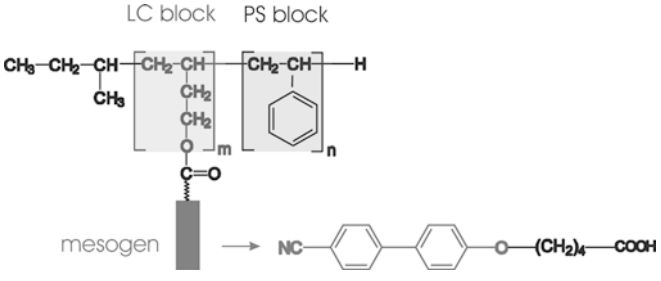

Fig. 1 Chemical structure of the PSLC block copolymers: the liquid crystalline block consists of cyanobiphenyl mesogens coupled to poly(1,2-butadiene) through valeric acid spacers and the isotropic block is polystyrene

Table 1 Chemical characteristics of the synthesized PSLC block copolymers

LC/I block copolymer	MW	N_{PS}	N_{LC}	PS wt% Calculated	LC wt%	N_{LC}/N_{PS} Calculated	N_{LC}/N_{PS} Measured	PS vol.% Calculated	LC vol.%
PSLC 7/93	77,000	42	208	5.7	94.3	4.95	[a]	6.8	93.2
PSLC 14/86	53,700	58	133	11.5	88.5	2.29	2.25	13.5	86.5
PSLC 19/81	104,300	163	250	16.3	83.7	1.53	[b]	19.0	81.0
PSLC 30/70	98,700	243	207	25.9	74.1	0.8518	[b]	29.6	70.4
PSLC 39/61	55,000	175	99	34.5	65.5	0.5657	0.553	38.8	61.2
PSLC 59/41	38,300	200	50	54.4	45.6	0.25	0.225	58.9	41.1
PSLC 77/23	62,800	444	48	73.4	26.6	0.1081	0.102	76.8	23.2
PSLC 85/15	86,500	662	42	82.5	17.5	0.0634	0.059	85.0	15.0
PSLC 97/3	125,000	1167	11	96.9	3.1	0.0094	0.014	97.4	2.6

[a]It was not possible to perform a measurement in the same solvent as the other block copolymers
[b]Measurements were not carried out

The absence of low-molecular weight impurities (e.g., unbound mesogen units) was also confirmed. The larger deviation of the experimental N_{LC}/N_{PS} values from the calculated ones for the block copolymers with the most asymmetric compositions as well as the inability to measure the block copolymer with the lowest PS content are attributed to the poor solubility of the two blocks in one and the same solvent. Polarized microscopy was done using an Olympus 41 optical microscope equipped with Linkam heating stage and a Eurotherm temperature controller with precision of ± 0.1 °C.

Wide and small angle X-ray scattering (WAXS and SAXS) The WAXS measurements were performed using X'Pert-PRO Philips set up with Spinner stage at 25 °C. Cu Kα radiation of wavelength 0.154 nm was selected by a curved crystal pyrolytic graphite monochromator. Two solar slits of 0.04 rad, one in the incident and one in the diffracted beam optics, were used to control the axial divergence of the X-ray beam. The slit-smeared scattering profiles were registered by a sealed proportional detector. Samples representing solid homogeneous disks with diameter of 13 mm and height of 1–2 mm were prepared by pressing the block copolymer powder in a special steel tool. The scattering vector is $q = \frac{4\pi}{\lambda}\sin\theta$ (2θ is the scattering angle) and the position of the first peak is denoted as q^*.

The SAXS diffraction profiles were measured in vacuum using a Kratky compact small angle system (PAAR, Graz, Austria) equipped with a step-scanning scintillation counter and a source of Cu Kα radiation of wavelength 0.154 nm. Temperatures of 25 to 170 °C were stabilized with a precision of ± 0.1 °C. At each temperature the sample was equilibrated for 30 min before starting the measurement. Details on the experimental equipment and sample preparation can be found in [21]. The recorded slit-smeared SAXS profiles were subjected to subtraction of the background scattering, normalization and desmearing using a special computer program based on standard procedures [22]. The normalization of the scattering intensity to the incoming X-ray flux measured with the moving slit device (PAAR, Graz, Austria) results in the absolute intensity in units of the Thompson cross section as a function of the scattering vector q.

Results and analysis

Nematic LC mesophase

The thermotropic LC behavior of the studied PSLC block copolymers was first probed by DSC and polarized microscopy. The DSC thermograms (see [21]) provided data for the nematic-isotropic transition temperature, T_{NI}, of the LC block as well as for the glass transition temperatures, T_g, of both copolymer blocks (except for the blocks with lowest volume fraction). Both glass transition temperatures are well separated confirming the microphase-separated state of the block copolymers and the existence of domain structure. The thermotropic LC behavior of the PSLC block copolymers is depicted in Fig. 2 and is generally characterized by the sequence g/~35 °C/n/~115 °C/i. Only for PSLC 97/3, the block copolymer with the lowest LC volume fraction, T_{NI} could not be detected. However, polarized microscopy revealed also in this case the presence of birefringent texture similar to those of the other block copolymers. Thus both DSC and polarized microscopy data proved the presence of a nematic LC mesophase at temperatures below T_{NI} for all PSLC block copolymers studied.

A characteristic length-scale of the nematic LC mesophase is the average distance between the nematic mesogens, d_N. It was studied by wide angle X-ray scattering. The WAXS profiles for all PSLC block copolymers as well as for the two homopolymers (LC and PS) at 25 °C are shown in Fig. 3a. In order to be able to

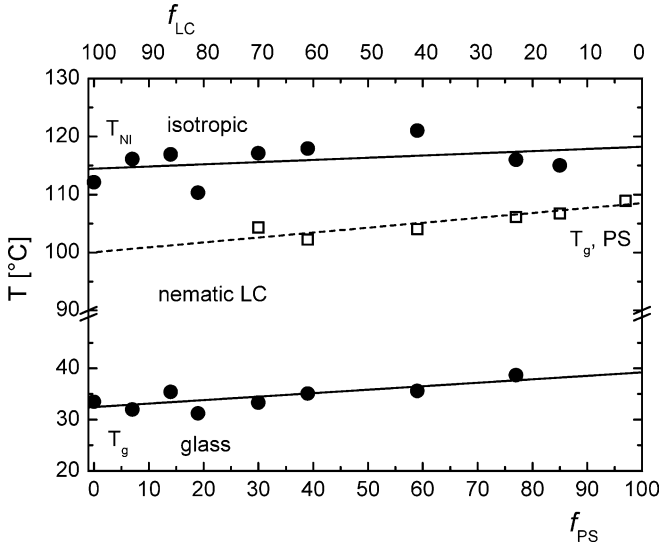

Fig. 2 Thermal characteristics (glass transition temperatures and LC mesomorphic behavior) of the PSLC block copolymers obtained by DSC

analyze the block copolymer profiles, we will first consider the characteristics of the two homopolymer profiles.

The profile of the PS homopolymer (Fig. 3b, bottom) features a main high intensity relatively narrow peak at $q^* = 13.59$ nm^{-1} and lower intensity peaks at $q = 7.15$ nm^{-1} and $q = 29.2$ nm^{-1}. It is identical to the PS scattering profile given, e.g., in [23]. It has been shown [24] that the scattering pattern at $q > 10$ nm^{-1} coincides with that of benzene and styrene. This indicates that, similarly to the monomer, the PS scattering profile in this q-range is dominated by the phenyl-phenyl correlations and represents scattering due to intrachain as well as interchain phenyl interactions [24]. The lower intensity peak at $q = 7.15$ nm^{-1} is completely absent in the monomer scattering profile and is identified with interchain correlations between first neighbors [24]. The analysis of this peak has revealed the spatial organization of the PS macromolecules in the glass state showing that the phenyl groups of neighboring macromolecules undergo microsegregation and associate into stacks [24]. This peak is specific to PS and is not present in the scattering profiles of most other polymers. A fit of the first two peaks of the PS profile as a superposition of two Gaussian peaks is shown in Fig. 3b.

The profile of the LC homopolymer (Fig. 3b, top) has quite the same characteristics, i.e., a high intensity relatively narrow main peak at $q^* \approx 14.5$ nm^{-1}, a lower intensity peak at $q = 29.5$ nm^{-1} (or approx. $2q^*$) and a hump to the left of the main peak. It is expected that, the scattering profile in this case is also determined by the intra- and interchain carbon-carbon correlations between first neighbors. However, an essential component of the profile here is the scattering due to the nematic LC mesophase. Despite the similarity between the X-ray scattering from LC homopolymer and from PS, the two profiles differ significantly with respect to the first peak. In the PS profile the peak at the lowest q is well-built. The presence of only a slight hump in the same q-range in the LC homopolymer profile indicates that the interchain correlations are entirely dominated by the

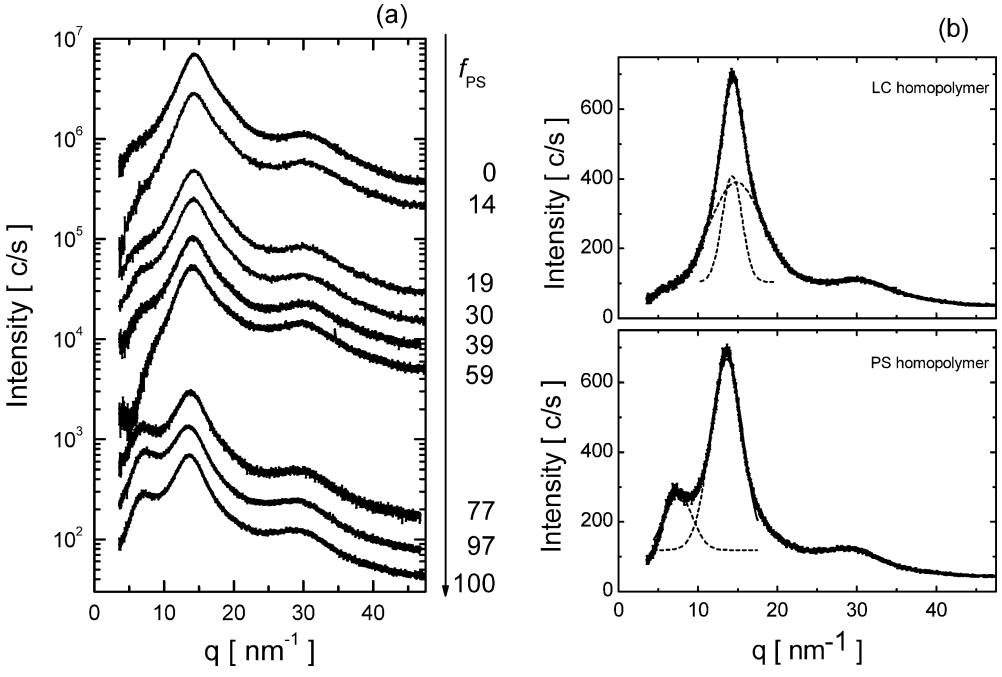

Fig. 3a,b WAXS diffraction profiles measured at 253: **a** for each of the PSLC block copolymers and for the two homopolymers, LC and PS; **b** comparison of the LC homopolymer profile to the PS homopolymer one. The profiles are shifted for clarity

scattering from the nematic LC mesophase, which appears at q values of the main peak.

The main peak of the LC profile itself is a superposition of two components. One is due to the scattering from the nematic mesophase and one is due to the "pure" intrachain carbon-carbon correlations. A useful method for assessing the structural origin of the profile features is the variation of the WAXS profiles with temperature. At temperatures below T_{NI} good fits of the main peak can be obtained only if it is considered as a superposition of two peaks (fit shown in Fig. 3b, top). The fits determine one relatively narrow strong peak resulting from the nematic mesophase and one broader lower peak from the "pure" intrachain correlations between first neighbors. At temperatures higher than T_{NI} good fits can be obtained by only one Gaussian peak. This outcome originates from the fact that above T_{NI} the nematic mesogens are not ordered and the resultant peak broadens and decreases in intensity. From the position of the first narrower peak in the scattering profiles at temperatures below T_{NI}, the distance between the nematic mesogens in the LC mesophase was calculated as $d_N = 0.44$ nm. This result coincides with literature data for LC polymers having similar biphenyl mesogens [14, 25, 26, 27].

Although it was still possible to distinguish the main peak positions in the LC and the PS homopolymer profiles, it was impossible to discriminate them superimposed in the profiles of the PSLC block copolymers. Here, analysis of the trends in the primary peak position can be helpful. Data for q^* determined by single Gaussian fits within equally wide q range for each PSLC block copolymer as a function of the PS volume fraction are given in Fig. 4. The q^* values gradually decrease from the value of the LC homopolymer to that of the PS homopolymer with increasing the PS content. However, the changes in the q^* value are smaller at higher LC content (from the LC homopolymer up to PSLC 59/41) and larger at higher PS content (from the PS homopolymer up to PSLC 59/41). Also, the q^* value changes only slightly between PSLC 39/61 and PSLC 59/41 (the shaded interval in Fig. 4 where the content of the LC block and the PS block is comparable). In this interval the PSLC profiles transform from predominantly PS one to predominantly LC one. Another clear tendency is the decrease of the prepeak intensity with decrease of the PS volume fraction, its disappearing at PSLC 59/41, and finally its conversion in a hump at the block copolymers with lower PS (higher LC) content. In this context, the WAXS profiles as presented in Fig. 3a demonstrate the continuous conversion of the characteristic features of the PSLC block copolymers profiles from those of the PS homopolymer to those of the LC homopolymers with decreasing the PS content.

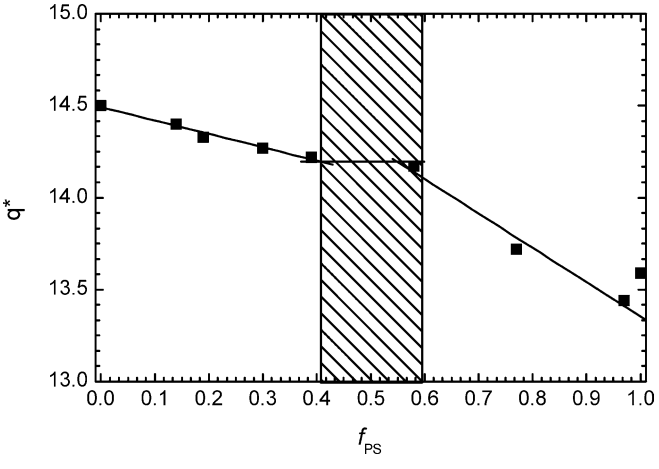

Fig. 4 Position of the primary peak in the PSLC block copolymer WAXS profiles as a function of the PS volume fraction

Here the calculation of d_N for the PSLC block copolymers as $2\pi/q^*$ is not correct because it is not possible to isolate that component of the main peak which results from the nematic LC mesophase. However, since the q^* value for the block copolymers from the LC homopolymer up to PSLC 59/41 varies within only 2%, and even the further larger change is within 8% (see Fig. 4), we can conclude almost with certainty that the distance between the mesogens does not significantly depend on the content of the LC block.

Domain microstructure

Various microdomain morphologies are attained by the PSLC block copolymers as a result of the block microphase separation and in dependence of the block volume fraction ratio. The characteristic length-scales of the domain microstructures were determined through analysis of the corresponding desmeared SAXS diffraction profiles. Several facts prove the microphase-separated state of the block copolymers. First, two distinct glass transition temperatures corresponding to the two blocks of the copolymers (Fig. 2) are registered in the DSC thermograms (with the exception of those with the lowest LC or PS content). Second, no order-to-disorder transition (ODT) was detected at any of the block copolymers up to 170 °C. In all cases the T_{ODT} is higher than the experimentally accessible temperature range. The rather high T_{ODT} is expected owing to the significantly high molecular weight of the block copolymers and the strong chemical dissimilarity of the blocks. Third, all registered scattering profiles show the presence of a number (in most of the cases 3 to 4) of relatively narrow diffraction peaks. These evidences indicate as well that the block copolymers are in the strong segregation regime [28, 29].

Lamellar microstructure

The desmeared SAXS profiles of the PSLC block copolymers of lamellar microstructure are shown in Fig. 5. The one-dimensional lamellar microstructure consists of alternating layers of the two blocks and is the simplest one to be established and analyzed. Three to four narrow high intensity Bragg peaks with positions relating as 1:2:3:4 can be distinguished in each profile. In the case of PSLC 77/23 additional three higher order peaks of weak intensity at positions $4q^*$, $5q^*$, and $6q^*$ are registered. To determine the precise q position of each peak, a Gaussian fit was used (shown in Fig. 5 as lines). Information for the lattice constant, i.e., the lamellae repeat distance, d, can be directly obtained by taking $2\pi/q^*$. Here, we present an alternative method developed initially for analysis of partially crystalline polymers by Strobl [30]. This method consists in calculation of the one-dimensional correlation function $K(z)$ as given by Eq. (1). It was chosen because it allows direct determination of the thickness δ of the thinner layer and gives important additional information about the interface between the two layers:

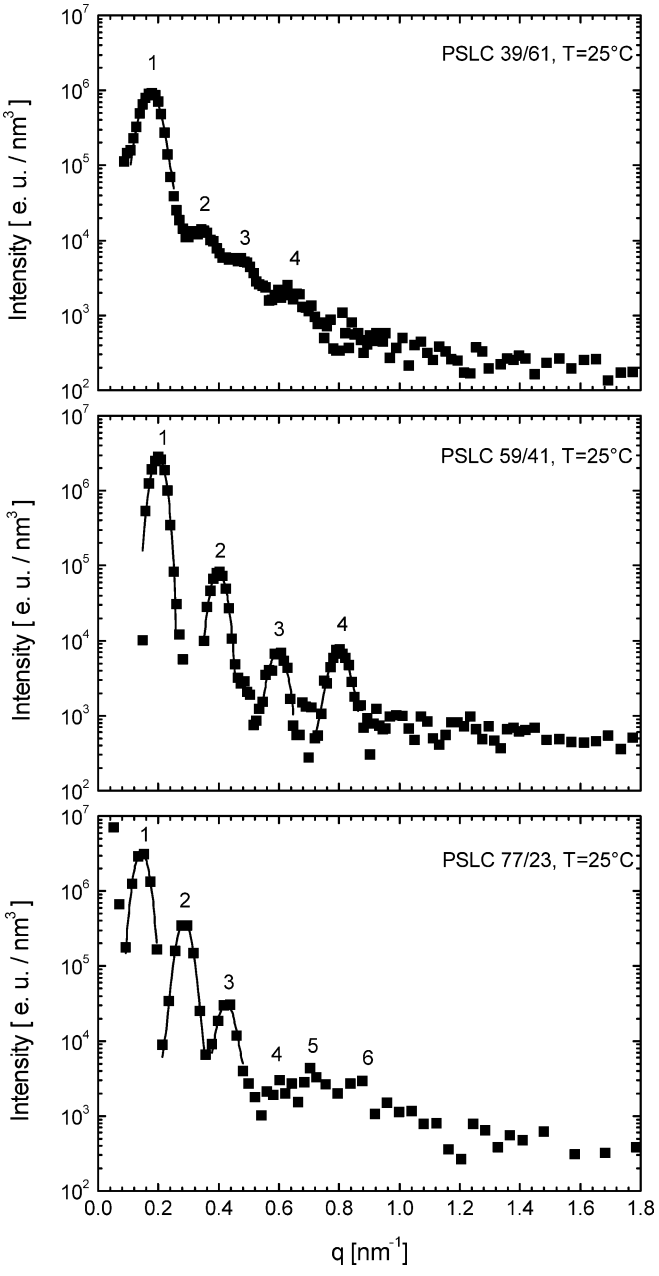

Fig. 5 Desmeared SAXS scattering profiles of the PSLC block copolymers having lamellar microstructure at 25 °C. Experimental data are given by points and the Gaussian fits of the diffraction peaks by lines

$$K(z) = \frac{1}{2r_e^2\pi^2}\int_0^\infty \cos(qz)q^2I(q)dq \qquad (1)$$

In Eq. (1) q is the length of the scattering vector, r_e is the classical electron radius, and z is the distance in direction normal to the lamellae surface. In order to calculate correctly this function from the experimental data, subtraction of the background and the scattering due to density fluctuations was done after Lorenz correction of the intensity.

The calculated correlation functions are given in Fig. 6. The lattice constant d is derived from the position of the first maximum. The thickness δ of the thinner layer (PS or LC layer depending on the composition) equals the x-coordinate of the intercept between the straight line fitting the initial part of the curve and the horizontal tangent to the first minimum. The values of the lattice constant so obtained agree within the experimental error with the values obtained directly by taking $2\pi/q^*$. The data are summarized in Table 2.

The shape of the correlation function characterizes the interface between the two layers. In the case of perfectly well-shaped and ordered lamellae with sharp interfaces the function consists of triangular peaks of equal height at equal intervals [30]. The correlation function for the present three PSLC block copolymers, however, represents a damped oscillation (Fig. 6). Such deviation in the shape of the correlation function indicates variations in the thickness of both layers [30]. Larger variations in the thickness of the thinner layer are observed in the case of PSLC 39/61, while for PSLC 59/41 and PSLC 77/23 larger variations appear in the thickness of the thicker layer. The above observation expressed in terms of LC and PS layers (compare the block volume fractions) shows that in all cases the PS layer thickness varies more significantly than the LC layer thickness. Deviations of the initial interval from linearity indicate gradual instead of sharp interface [30]. As is seen, in all cases the initial interval is fairly linear implying a rather sharp interface between the LC and

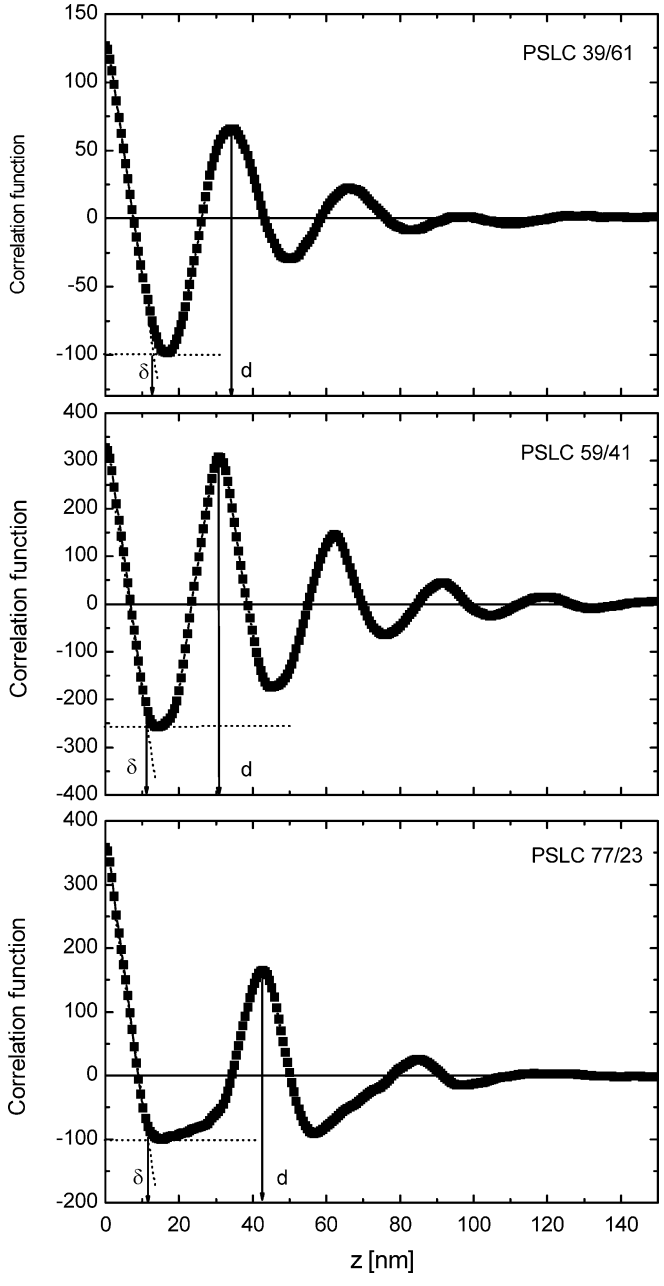

Fig. 6 Correlation function of the SAXS scattering profiles of the PSLC block copolymers of lamellar microstructure

the PS layers, which is expected in the strong segregation regime. This result is consistent with the conclusions of Fischer et al. [16] and Ober et al. [15] for smectic LC/PS block copolymers.

Hexagonal microstructure

The two-dimensional hexagonal microstructure consists of cylindrical domains of one copolymer block ordered in a hexagonal lattice situated in continuous matrix of the other block. The scattering profiles of the hexagonal microstructures are presented in Fig. 7. Several Bragg peaks over a significant diffuse scattering component are recognized in all scattering profiles. In this case a quantitative description is obtained by fitting the scattering profiles to a theoretical model describing the scattered intensity as a sum of three components: (i) Bragg reflections from the LC microstructure modulated by the form factor of the scattering microdomains; (ii) diffuse scattering from the positional disorder and the size distribution of the microdomains; and (iii) background scattering from density fluctuations [18, 31, 32]:

$$I(q) = I_{Bragg} + I_{diff} + I_k \tag{2}$$

The contribution of the Bragg reflections to the scattered intensity at scattering vector q in a non-oriented sample is given by [31]

$$I_{Bragg} = \sum_{\{hkl\}} \overline{\Phi^2}(q_{hk}) \frac{j_{hk}}{q^2} G_{hk}(q;\sigma) \exp\left\{-q_{hk}^2 u^2/3\right\}, \tag{3}$$

where $1/q^2$ is the Lorenz factor for an isotropic distribution of the domains, $\{hk\}$ are the Miller indices of the reflections characteristic of the hexagonal lattice, j_{hk} is the multiplicity of reflection $\{hk\}$, and $G_{hk}(q;\sigma)$ is a normalized Gaussian function centered at q_{hk} with variance of σ. The peak position q_{hk} is directly related to the lattice constant a [31]:

$$q_{hk} = \frac{2\pi}{a}\sqrt{\frac{4}{3}(h^2 + k^2 + hk)} \tag{4}$$

The form factor of the cylindrical microdomains Φ has to be also considered since it varies in the q interval of investigation [31, 33]. It is spatially averaged to account for the isotropic arrangement of domains in the sample:

$$\Phi(q) = 2V \int_0^{2\pi} \frac{\sin\left(\frac{qL}{2}\cos\alpha\right)}{\frac{qL}{2}\cos\alpha} \frac{J_1(qR\sin\alpha)}{qR\sin\alpha} d\alpha \tag{5}$$

where V, L, and R are respectively the volume, the length, and the radius of the cylinders, J_1 is the first order Bessel function, and α is the angle between the cylinder axis and the scattering vector q. The exponent in Eq. (3) represents the Debye-Waller factor. Its physical origin is the deviation of the location of the individual scattering objects from their equilibrium position. The mean squared displacement is u^2. This type of lattice distortion gives also rise to a diffuse scattering I_{diff}. [18]:

$$I_{\text{diff}} \propto \left(1 - \exp\left(q^2u^2/3\right)\right)\overline{\Phi}^2 + \left(\overline{\Phi^2} - \overline{\Phi}^2\right). \tag{6}$$

Table 2 Microstructure characteristic length-scales (d, a, δ, R) obtained from the fits

LC/I block copolymer	Microstructure	Morphology	l [°C]	d, a [nm]	δ,R [nm]
PSLC 7/93	Hexagonal	PS cylinders in LC matrix	25	33.6 ± 0.1	4.5 ± 0.2
PSLC 14/86	Hexagonal	PS cylinders in LC matrix	30	27.4 ± 0.1	5.5 ± 0.1
PSLC 19/81	Hexagonal	PS cylinders in LC matrix	25	46.6 ± 0.2	13.0 ± 0.1
PSLC 39/61	Lamellar	PS and LC lamellae	25	34.2 ± 0.6	12.8
PSLC 59/41	Lamellar	PS and LC lamellae	25	30.9 ± 0.1	11.2
PSLC 77/23	Lamellar	PS and LC lamellae	25	42.8 ± 0.1	11.2
PSLC 85/15	Hexagonal	LC cylinders in PS matrix	25	41.7 ± 0.1	6.6 ± 0.3
PSLC 97/3	bcc	LC spheres in PS matrix	30	38.3 ± 1.0	4.7 ± 0.8

The last term—I_k in Eq. (2)—represents the background due to density fluctuations. The fits to the experimental profiles are also shown in Fig. 7. It is obvious that in each case the theoretical model describes very well the experimental data. The lattice constant, a, the radius of the cylinders, R, as well as information for the degree of lattice order are directly obtained. The data are summarized in Table 2.

PSLC 30/70—on the border between the hexagonal and lamellar microstructures

The diffraction profile of PSLC 30/70 (Fig. 8) could not be assigned unambiguously to a given microstructure at any of the temperatures studied (25 °C up to 150 °C). Its total intensity is high and comparable to that of the neighbors PSLC 19/81 (hexagonal microstructure) and PSLC 39/61 (lamellar microstructure). Two weak peaks can be recognized over a very strong diffuse scattering. As discussed in the beginning of this section, PSLC 30/70 is in the microphase-separated state similarly to the other block copolymers. However, the strong diffuse scattering component implies that the microdomains are irregular and/or poorly ordered. The positions of the two peaks relate approx. as 1:2.5. This ratio is closer to $1 : \sqrt{7}$ than to 1:2 or to 1:3, which allows one to exclude the lamellar microstructure as the only one present. On the other hand, the fit of the diffraction profile to a hexagonal microstructure using the model described above (Eqs. 2, 3, 4, 5, and 6) did not give a satisfactory result (the best possible fit is given in Fig. 10 as a line).

Another option is to assume a bicontinuous cubic microstructure. Such structures are very rare in one component LC/I block copolymer systems [15, 19]. They appear between the hexagonal and lamellar structures and give profiles of high intensity as in this case. However, in contrast to the present case, they are expected in the weak segregation regime [4]. The attempt to fit the diffraction profile of PSLC 30/70 to a bicontinuous cubic structure also failed.

Therefore, we are led to assume that we have a mixed lamellar-hexagonal structure or a complex structure of perforated lamellae with cylindrical inclusions of rectangular symmetry [17]. The strong diffuse scattering indicates large lattice distortions and, thus, exclude a pure structure with high regularity. It is concluded that PSLC 30/70 most probably lies exactly at the border between the hexagonal and lamellar microstructures and have a mixed structure with large domain disorder in the studied temperature range. Our attempt to "cure" the structure and attain a pure one by annealing the sample above T_{NI} at 120 °C for 24 h under vacuum was however unsuccessful most probably due to the extremely slow kinetics of the process.

Cubic microstructure

The diffraction profile of PSLC 97/3, the block copolymer with the lowest LC content, is shown in Fig. 9. It is characterized by a significantly low intensity: about one order of magnitude lower than the neighboring PSLC 85/15 and more than one-and-a-half orders of magnitude lower than the PSLC 30/70 discussed above. The PSLC 97/3 profile features only one peak and a relatively strong diffuse scattering component. These characteristics indicate that the microdomains are poorly ordered. At such a low content of one of the blocks, it is reasonable to suppose that the structure is a micellar cubic one. The three-dimensional micellar cubic microstructures consist of spheres of one copolymer block ordered in a cubic lattice into matrix of the other block. Their diffraction profiles are usually of quite low intensity. Since in one-component block copolymer systems the body-centered cubic (bcc) lattice is the most often present one, we have fitted the profile to a bcc structure using the model described above (Eqs. 2, 3, 5, and 6). At this we have substituted the Miller indices of the reflections characteristic of the hexagonal lattice, $\{hk\}$, with the corresponding Miller indices for the bcc structure, $\{hkl\}$, and using their multiplicities j_{hkl} we have summed up over all possible reflections (Eq. 3). In Eqs. (5) and (6) the form factor of the cylindrical microdomains was substituted by the form factor of spherical domains with volume V and radius R (Eq. 7) [34]. The fit is shown in Fig. 9 (top). It is obvious that the model fits well the experimental data. The data obtained for the lattice

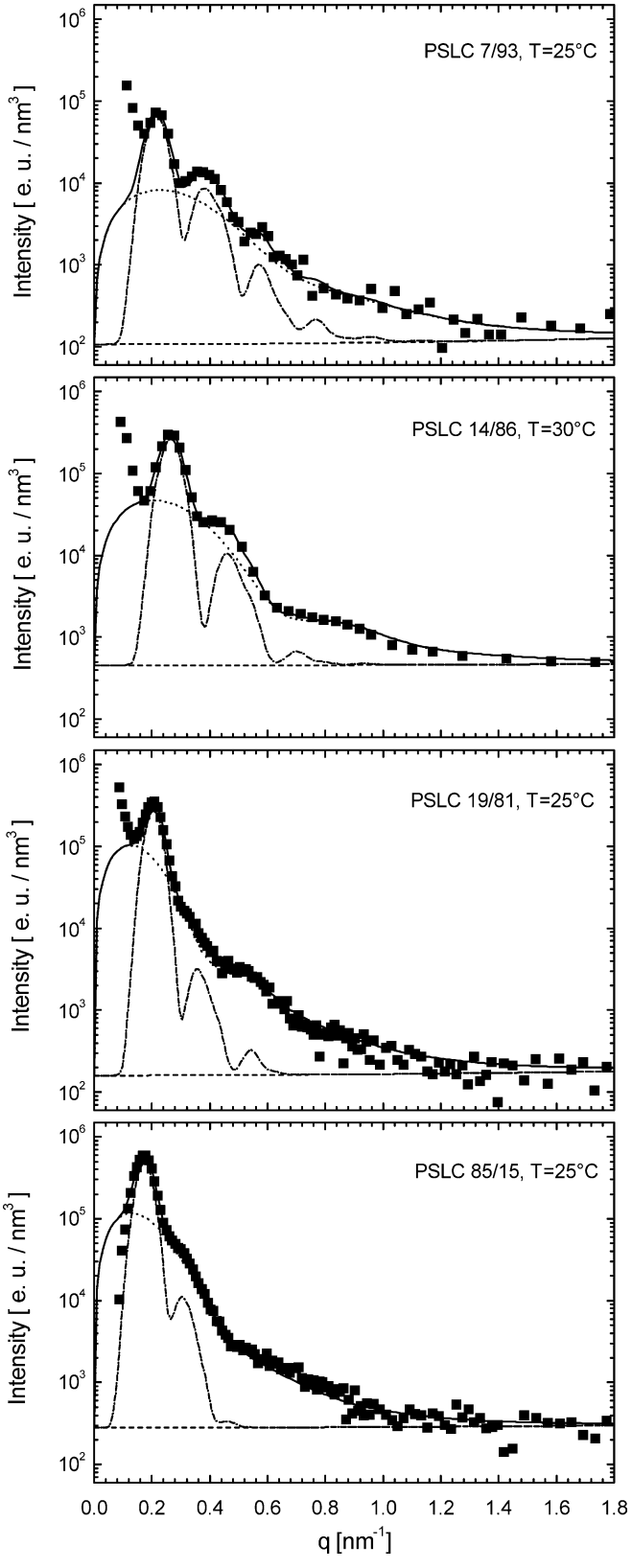

Fig. 7 Desmeared SAXS scattering profiles of the PSLC block copolymers having hexagonal microstructure at 25 °C. The data for PSLC 14/86 are taken at 30 °C. The experimental data are given by *points* and the fits by *solid lines*. The *dashed lines* represent the three component of the scattered intensity. The same notation is used in Fig. 10 and Fig. 11

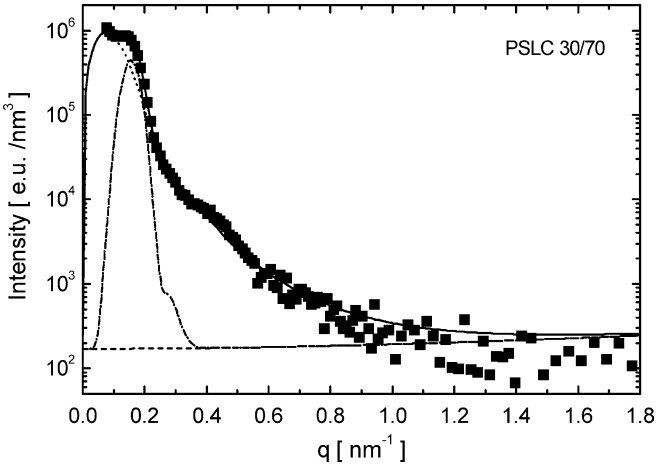

Fig. 8 Desmeared SAXS scattering profile of PSLC 30/70 at 25 °C. The best fit (*full line*) to hexagonal microstructure is also shown. *Broken lines* are components of the scattering intensity (see text)

constant, a, and the radius of the spheres, R, are given in Table 2:

$$\Phi(q) = 3V\frac{\sin(qR) - qR\cos(qR)}{(qR)^3}. \tag{7}$$

Despite the good agreement of the experimental data to the bcc model, the presence of only one Bragg peak in the profile can possibly imply that the spherical domains are not strongly correlated and display a liquid like order. As has been shown earlier [32, 35], such structures are found for asymmetric diblock copolymers between the disordered and the bcc ordered state. They are well described by the Percus-Yevick approximation of "hard sphere" liquid. The scattered intensity is then given by

$$I(q) = K\overline{\Phi^2}(q)S(q,R,\eta) + I_k, \tag{8}$$

where the prefactor K depends on the scattering contrast between the LC and the PS block, Φ^2 is the form factor of the spherical domains (Eq. 7) averaged over their size distribution by a Gaussian function [32], $S(q,R_{\mathrm{hs}},\eta)$ is the interference factor, R is the radius of the spherical domains, R_{hs} is the hard sphere radius representing the effective interaction distance, η is the effective hard sphere volume fraction, and I_k is the scattering background due to density fluctuations. An explicit expression of the interference function $S(q,R_{\mathrm{hs}},\eta)$ is given in [32].

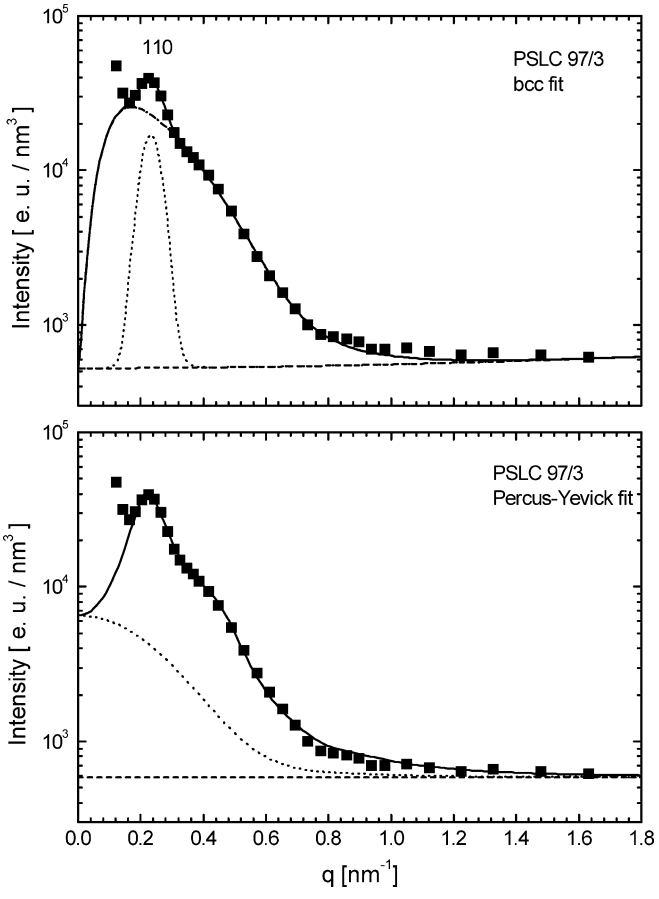

Fig. 9 Desmeared SAXS scattering profile of PSLC 97/3 at 30 °C. Both fits by the bcc model (*top*) and by the Percus-Yevick model of "hard sphere liquid" (*bottom*) are presented

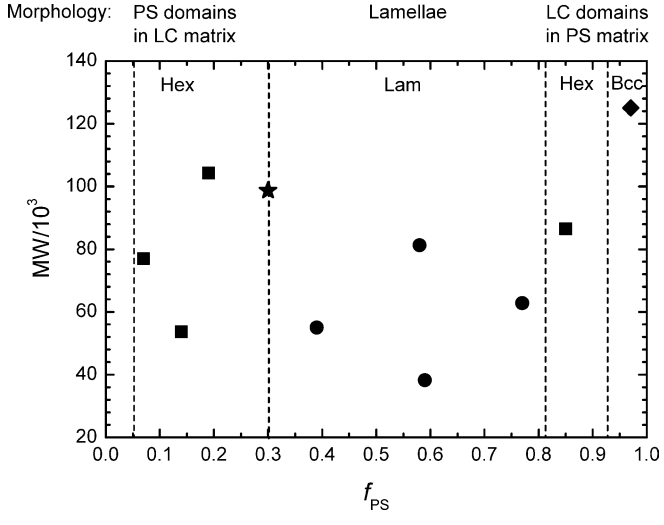

Fig. 10 Phase diagram of the PSLC block copolymers. Different symbols are used for different domain structures

The fit of the experimental data to the theoretical function (Eq. 9) is shown in Fig. 11 (bottom). It is obvious that this model also describes well the scattering profile. Moreover, the radius of the spherical microdomains obtained by the Percus-Yevick model ($R = 4.8 \pm 0.1$ nm at 30 °C) coincides within the experimental error with the value obtained by the bcc model ($R = 4.7 \pm 0.8$ nm). The equal quality of the two models shows that the PSLC 97/3 microstructure is neither that of dilute spheres nor that of a well ordered bcc lattice. Rather, it has to be considered as both a largely disordered bcc lattice or an ordered liquid of spheres. It can be speculated that the large error of the domain radius determined by the bcc model (Fig. 11, bottom) is a result of ellipsoidal instead of spherical domains. The bcc model would see equally ellipsoidal domains and spherical domains with large polydispersity. In the following we consider the results from the fit to the bcc model.

Structure morphology and phase diagram

The phase diagram of the studied LC/I block copolymers shown in Fig. 10 was build on the basis of the domain microstructures as identified above. The diagram displays the phase behavior in terms of the molecular weight of the block copolymers in dependence on the composition. Since the domain microstructures remain unaffected at all studied temperatures, below as well as above T_{NI}, the molecular weight scale can be rescaled in terms of $N\chi$ or temperature, N being the total degree of polymerization and χ the interaction parameter. Assuming that $N\chi$ is sufficiently large, the estimated phase boundaries are independent of the composition an therefore are depicted as vertical lines. Despite the limited number of block copolymers, we believe that no essential mistakes are made in delineating the phase boundaries in the studied molecular weight range thanks to the systematic variation of the block volume fractions. The phase diagram is asymmetric and characterized by a broad lamellar structure dominating over the entire composition range. Hexagonal microstructure of morphology PS cylinders in LC matrix is the next favored. The formation of cubic microstructures is strongly suppressed. In summary, structures of low interfacial curvature (lamellar and hexagonal) are favored at the expense of structures of high interfacial curvature (micellar cubic). Structures where the LC block is located in the matrix (on the convex side of the interface) are preferred over structures having the LC block inside the microdomains (LC cylinders or spheres in PS matrix). This result confirms the theoretical prediction by Hammond et al. [13].

The type of the nematic mesophase formed in the matrix or inside the domains depends on the mutual

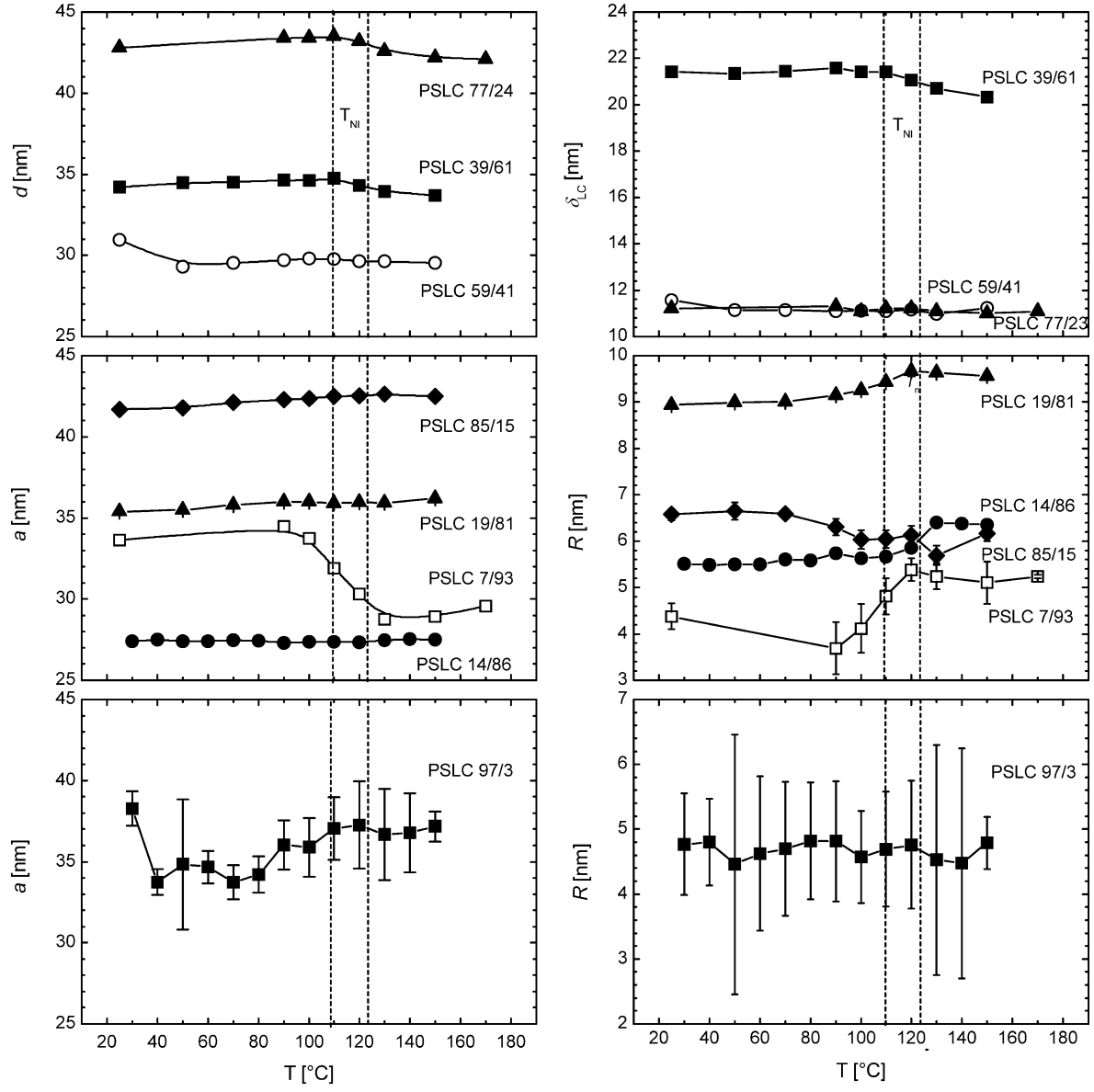

Fig. 11 Temperature dependence of the microstructure length-scales: (*left*) lattice parameter, d or a and (*right*) domain dimensions, δ or R; (*top*) lamellar structures, (*middle*) hexagonal structures, (*bottom*) cubic structure. The T_{NI} interval is denoted by *two dashed lines*

orientation of the LC backbone, the mesogens, and the interface [13, 36]. It is difficult to be identified only on the basis of the present experiments. Most probably the anchoring is planar, i.e., the LC backbone is stretching away normal to the interface and the nematic director is parallel to the interface. An indication is the slight variation in the lattice parameter in the lamellar microstructures at the T_{NI} temperature (discussed below). The planar anchoring is the most frequently present in similar systems [25]. It has been found that as a rule mesogens attached to the backbone chain through long spacers form smectic phases which can be both planar or homeotropically anchored, while mesogens with short spacers form mainly nematic phases with planar anchoring [14].

Temperature dependence of the domain dimensions

The fitting procedures (see above) were applied for each PSLC block copolymer to all SAXS diffraction profiles registered in the temperature range 25–170 °C in the heating and cooling runs. The lattice constant obtained (d in the lamellar or a in the hexagonal and cubic structure) as well as the microdomain size (the LC layer thickness, δ_{LC}, or the radius of the cylinders/spheres, R)

upon cooling are shown in Fig. 11. In the entire temperature range the lattice constant for the block copolymers with exception of PSLC 7/93 does not vary or varies only slightly. The data in the cubic structure are obtained with significant error and cannot be analyzed reliably.

In the lamellar microstructure the lattice parameter increases slightly with increasing the temperature up to T_{NI} and then slightly decreases (Fig. 11, top). The initial increase in the domain dimensions is a result of the thermal expansion of the macromolecule. It is to be expected that this process will continue also above T_{NI}. In order to understand this apparent discrepancy, we evaluate the effect of variation of the layer thickness δ on the degree of polymerization N for PS and LC assuming a power law behavior $\delta \propto N^{\gamma}$. For the PS domain we find $\gamma_{PS} = 0.8 \pm 0.2$ at all temperatures. A value of 0.8 is expected for I/I block copolymers in the intermediate regime and a value of 2/3 in the strong segregation regime [28, 29]. Since the scaling power was obtained with a significant error, unambiguous identification of the segregation regime was not possible. The LC layer thickness, however, scales with $\gamma_{LC} = 0.92 \pm 0.05$ up to T_{NI}. This implies larger stretching of the LC backbone chain. This outcome is a consequence of the NI type of the nematic mesophase for the investigated side-chain LC polymer and the planar anchoring of the mesogens at the interface [37, 38] leading to an oblate chain conformation with respect to the nematic director, i.e., to enhanced stretching of chains perpendicular to the interface [13]. At temperatures higher than T_{NI} the scaling power decreases and reaches $\gamma_{LC} = 0.85 \pm 0.02$ at 150 °C. The disordering of the nematic mesogens in this range allows the backbone to retract from its entropically unfavored stretched conformation and leads to the observed decrease of the domain dimensions. The scaling power of the LC block then approaches that of the PS block. The conformation of the LC chain is a result of the competition between the entropy of the chain on one hand and the nematic field on the other hand. Similar results for the lamellar domain spacing have been obtained in related LC/I block copolymer systems [25, 39, 40].

The variations in the domain dimensions in the hexagonal microstructure will be discussed only qualitatively. A significant change in the lattice constant and a corresponding reverse change in the cylinder radius take place only at PSLC 7/93 (Fig. 11, middle). This is the polymer with the lowest PS content and presumably lays near to the border of the hexagonal structure in the phase diagram (as depicted in Fig. 10). The observed change indicate a tendency to undergo an order-to-order transition from hexagonal to cubic microstructure triggered by the nematic-to-isotropic transition. Such transition is energetically determined because at temperatures higher than T_{NI} the elastic energy arising from nematic field distortions [41] is excluded from the energy balance. This will allow the domain shape to return to the equilibrium one expected for I/I block copolymers at such block volume ratio. Such a transition has been experimentally observed for a similar PS-LC-PS triblock copolymer with PS volume fraction of 0.141 [18]. In the present case, however, it was not possible to fit the scattering profiles recorded above T_{NI} to a cubic structure. Obviously here, the released elastic energy is not sufficient to cover the energy expenses for the domain transformation and they only rearrange. Above T_{NI} the PS domains expand (R increases), while the LC domains contract (a decreases) due to retraction of the LC backbone in the isotropic state.

The lattice constant for other three block copolymers with hexagonal structure practically does not vary with the temperature. However, the cylinder radius changes. In the cases of PSLC 14/86 and PSLC 19/81 R increases similarly to PSLC 7/93. For PSLC 85/15 R decreases. Having in mind that at PSLC 85/15 the cylindrical microdomains encapsulate the LC block, contrary to the other three copolymers, we arrive to one and the same conclusion. Above T_{NI} the PS domains continue to expand with T, while the LC domains retract.

Discussion

Influence of the domain microstructure on the nematic LC mesophase

With respect to the thermotropic behavior of the nematic mesophase, no specific influence of the LC content and, hence, the domain structure on T_{NI} can be detected (Fig. 2). However, with one exception (PSLC 19/81) there is a trend of elevated T_{NI} in the block copolymers with respect to the LC homopolymer. This may be an indication of stabilization of the LC phase due to confinement between PS cylinders, inside LC lamellae, or LC cylinders, respectively. However, there are not enough data available to allow a correlation to characteristic length scales. There is a trend of slight decrease of T_g with increasing the LC content, however independent on the domain structure. With respect to the intermesogen distance, d_N presumably does not depend on the content of the LC block as discussed above. It is concluded that the thermotropic LC behavior of the studied PSLC block copolymers is not influenced by the domain structure and/or domain dimensions.

Influence of the nematic LC mesophase on the domain microstructure

The effect of the nematic mesophase on the domain structure is much more pronounced. It is best expressed

in the characteristics of the phase diagram (Fig. 10) which significantly differs from experimental [4, 42] and theoretical [29] ones for I/I block copolymers even if the inherent conformational asymmetry of the LC/I block copolymers is taken into account (see below). Below T_{NI} the nematic mesophase present in the matrix or in the microdomains plays obviously an essential role. As has been mentioned, the phase diagram is asymmetric and structures of low interfacial curvature are dominant. The hexagonal microstructure of morphology PS cylinders in LC matrix persists down to less than $f_{PS} = 0.07$, contrary to the significantly higher value of 0.15 for I/I block copolymers. The physical reason is distortion of the nematic field in the vicinity of the domains. Spherical particles suspended in a nematic LC matrix lead to distortions of the nematic director which give rise to elastic forces between the particles [41]. In the present case the elastic forces are compensated by formation of cylindrical instead of spherical domains. Obviously, the energy penalty for the formation of cylindrical domains, having the next smallest free energy but better compatible with the nematic filed, is smaller than the elastic energy from the nematic field distortions by spherical domains. Similar reasons account for the broadening of the lamellar phase (up to $f_{PS} \backsim 0.82$ instead of 0.66) at the expense of hexagonal microstructure of morphology LC cylinders in PS matrix.

A comparison of the present phase diagram to the available literature data for other side-chain LC/I block copolymers [14, 15, 16, 17] shows that the phase diagram is specific to the mesogen type, the mesomorphic behavior and anchoring. The phase diagram of block copolymers with rather bulky cholesteryl mesogen [16] is, contrary to the present one, relatively symmetric and is characterized by a broad micellar cubic structures and a lamellar structure comparable to that in the I/I block copolymers in comparable molecular weight range. Another difference is the significant influence of the domain microstructure on the mesomorphic behavior expressed in formations of chiral nematic mesophase instead of smectic one in the morphology LC spheres in PS matrix. The phase diagram of block copolymers with similar to ours azobenzene mesogens is similar to the present one at high LC contents (PS domains in LC matrix morphologies) and differs at high PS contents in broad molecular weight range [14, 15]. Finally, a comparison to the phase diagram of block copolymers with the bulkier biphenyl benzoate mesogen shows similarly broad lamellar and hexagonal (PS cylinders in LC matrix morphology) microstructures in limited lower molecular weight range [17].

In a recent report by Hammond at al. [13], a free-energy model has been developed on the base of the Wang and Warner theory of nematic side-chain LC polymers [36] accounting for the competition between the polymer entropy and the nematic order. Four other terms are completing the free energy expression: (i) the stretching free energy of the isotropic block; (ii) the interfacial free energy; (iii) the elastic energy from nematic field distortions; and (iv) the Flory-Huggins mixing free energy. By minimizing the free energy of each domain microstructure, the theoretical phase diagrams have been computed. The influence of the mesogen anchoring (planar or homeotropic), the molecular weight, the mesogen-mesogen interactions and the substitution degree have also been investigated. For planar anchoring the authors have predicted an asymmetric phase diagram with large lamellar and hexagonal structure regimes and with isotropic cylinders in the LC matrix. As the authors have shown, it agrees well with the available experimental data [14, 15, 16, 17]. The model describes equally as well the present phase diagram with the exception of a slight disagreement at high LC content.

The authors have also shown [13] that at the isotropisation temperature of the LC mesophase, in the phase diagram for the case of planar anchoring there appear narrow windows allowing for order-to-order transitions between two domain morphologies of the type reported earlier [18, 19]. However, these effects do not bring the phase diagram closer to that of the I/I block copolymers. In fact, above T_{NI} the phase diagram remains strongly asymmetric although the nematic elastic energy is excluded from the energy balance. This prediction agrees very well with the present experimental phase diagram. The width of the transition windows depends on the mesogen type and becomes smaller with increasing interactions between the mesogens. Since each point in the phase diagram of one-component block copolymer systems represents a separate copolymer and means separate synthesis (hence no real fine tuning of the block volume faction is possible), the above result means that there is only quite small room for a given block copolymer where it has to be luckily located in order to undergo OOT. This readily explains why until now only few OOT have been reported [13, 18, 19].

Conformational asymmetry

The PSLC block copolymers are conformationally asymmetric by virtue of the long side chains of the LC block. Above T_{NI} in the isotropic melt, where no influence of the nematic phase is present, the phase behavior should then only be governed by the conformational asymmetry and we will attempt to compare the present results with theoretical predictions [43, 44]. The conformational asymmetry is characterized by the different monomeric volumes or densities ρ_{0i} and the different Kuhn lengths b_i of the components (i = PS, LC). Since melts are incompressible a common average monomeric volume $1/\rho_0$ can be introduced and both parameters can

be subsumed into statistical segment lengths a_i defined by $a_i^2 = (\rho_{0i}/\rho_0)b_i^2$. An asymmetry parameter can then be defined by the ratio of the segment lengths as $\epsilon = a_{PS}/a_{LC}$. This conformational asymmetry causes the phase diagram to be asymmetric. Generally micellar phases (cylinders, spheres) of the component with larger segment length are stabilized and broadened while the opposite is true for the other component, i.e., the phase boundaries are shifted toward higher volume fractions of the block with larger segment length ($\epsilon > 1$). The physical reason is that the entropy loss of the Gaussian chains due to the chain stretching is proportional to l^2/a^2 where l is the distance to which the segments are stretched. Therefore, in a lamellar morphology of an asymmetric block copolymer the entropy loss due to chain stretching perpendicular to the interface increases relative to the symmetric system when the volume fraction of the component with larger segment length decreases. A way to decrease the free energy is to relax the stretching of the block with the smaller segment length thus leading to a curved interface leaving the block of larger segment length on the concave side of the interface.

The experimental phase diagram in Fig. 10 shows that the hexagonal phase of PS cylinders is broadened while the width of the inverse hexagonal phase of LC cylinders is smaller. Therefore, we conclude that the PS segment length a_{PS} is larger than the segment length of the LC block ($\epsilon > 1$). By comparing the phase boundaries of the experimental phase diagram to phase boundaries calculated by self consistent field theory we can estimate the asymmetry parameter and from this we obtain the Kuhn length b_{LC} of the LC polymer. To do this we make use of the calculation by Matsen and Bates (Fig. 3 in [43]) where they calculated the phase boundaries between lamellar, cylindrical, spherical, and disordered phases as function of the conformational asymmetry for $\chi N = 30$, 60, and ∞, respectively. Knowing that $\epsilon > 1$ we obtain a consistent value of $\epsilon = 1.33$ from the upper and lower boundaries of the lamellar morphology ($f_{PS} = 0.38$, 0.78) for $\chi N = \infty$. Using the Kuhn length of polystyrene (0.68 nm) and the monomeric densities of PS (6.02 nm^{-3}) [44] and the LC polymer (2.16 nm^{-3}) we estimate a Kuhn length of 0.86 nm for the LC block. The value is of similar magnitude as for branched polymers, e.g., for poly(dodecyl)methacrylate (0.80 nm in theta-solvent pentanol) which has a similar number of linear C/O atoms in the side chain (14) as the LC block (18 linear C/N/O-atoms) and also has a similar monomer volume (0.454 nm^3) [45]. The fact that the boundaries between lamellar and cylindrical phases which are delineated in Fig. 10 do not give consistent results for the asymmetry parameter is probably due to the paucity of the data, possibly also due to some compositional range around $f_{PS} = 0.3$ which can neither be assigned to a lamellar nor to a hexagonal phase. The phase boundary between hexagonal LC cylinders and the LC bcc phase is predicted to occur at $f_{PS} = 0.95$ in close proximity to the estimated line in Fig. 10. It should also be noted that the boundary between PS cylinders and PS spheres is predicted to occur at $f_{PS} = 0.18$ which is in contradiction to the experimental observation. The hexagonal phase is found to persist at least down to $f_{PS} = 0.7$. As mentioned above the constraint imposed on the interfacial curvature by the nematic phase is released when passing into the isotropic melt and an OOT transition to the bcc phase can be expected. This transition has been observed by our group for a PS-LC-PS triblock copolymer with the same structure of the LC block at the same composition as the PSLC 14/86 diblock [18]. At this composition the release of constraints by the nematic field leads only to an increase of the domain dimensions of the PS cylinders which intensifies going to PS 7/93 (Fig. 11). It is noted that the latter block copolymer possesses almost twice the molecular weight as the equivalent diblock molecular weight of the triblock (42,000 g/mol) where the OOT was observed. Also the composition-equivalent PSLC 14/86 has significantly larger molecular weight. It can be conjectured that the observed dimensional changes at T_{NI} are signs of the onset of an OOT which is prevented to run to completion by kinetic hindrance due to molecular weight.

Conclusions

The thermotropic liquid crystalline behavior and the microdomain morphologies of nematic side-chain LC/I diblock copolymers have been studied. A nematic LC mesophase with characteristic length-scale of 0.43 nm and various domain microstructures with characteristic length-scale of 27–44 nm were identified and characterized by DSC, polarized microscopy and X-ray scattering. No influence of the domain microstructure and/or dimensions on the thermotropic LC behavior, characterized by the sequence g/$\backsim$35 °C/n/$\backsim$115 °C/i, was detected.

The reverse effect of the nematic mesophase on the domain microstructure was shown to be much more pronounced. The main impact is the asymmetric phase diagram which differs strongly from that of I/I block copolymers and, up to some extend, from that of other LC/I block copolymers. Due to the additional elastic energy arising from distortions of the nematic field, microstructures of low interfacial curvature (lamellar and hexagonal) are energetically preferred over geometrically expected ones of high interfacial curvature (micellar cubic). Microstructures of PS domains in a continuous LC matrix are favored. In general, the phase diagram is in agreement to the theoretical one for planar anchoring by Hammond et al. based on the Wang and Warner theory of nematic side-chain LC polymers.

At temperatures higher than T_{NI} the phase diagram remains unaffected and asymmetric. From the lamellar/hexagonal phase boundaries an estimate of the Kuhn length of the LC block is obtained by comparison to theoretical predictions for the effect of the conformational asymmetry. No order-to-order transitions triggered by the nematic-isotropic transition were registered. Analyzing the temperature effect on the domain dimensions and the block scaling in the lamellar microstructure showed that at low temperatures the LC chain is stretched. With increasing temperature, a thermal expansion of both blocks takes place (the domain dimensions increase). At temperatures higher than T_{NI} a retraction of the LC chain occurs (the domains dimensions decrease) as a result of ''the switching off'' the nematic field.

Acknowledgements The authors are grateful for the financial support of this study by the German Ministry of Education and Research (BMBF Grant 03STE3IL) and to the German Research Foundation (DFG).

References

1. Mortensen K (2001) Colloids Surf A 183/185:277–292
2. Alexandridis P, Lindman B (eds) (2000) Amphiphilic block copolymers: self-assembly and applications. Elsevier Science B.V., Amsterdam
3. Hasegawa H (1998) Curr Opin Colloid Interface Sci 3:264–269
4. Bates FS, Schultz MF, Khandpur AK, Förster S, Rosedale JH, Almdal K, Mortensen K (1994) Faraday Discuss 98:7–18
5. Ivanova R, Lindman B, Alexandridis P (2001) Adv Colloid Interface Sci 89/90 351–382
6. Ivanova R, Lindman B, Alexandridis P (2002) J Colloid Interface Sci 252:226–235
7. Alexandridis P, Spontak RJ (1999) J Curr Opin Colloid Interface Sci 4:130–139
8. Lehmann W, Skupin H, Tolksdorf C, Gebhard E, Zentel R, Krüger P, Lösche M, Kremer F (2001) Nature 410:447–450
9. Terentjev EM (1999) Curr Opin Colloid Interface Sci 4:101–107
10. Walther M, Finkelmann H (1998) Macromol Rapid Commun 19:145–148
11. Fischer H, Poser S (1996) Acta Polym 47:413–428
12. Mao G, Ober CK (1997) Acta Polym 48:405–422
13. Anthamatten M, Hammond PT (2001) Polym Sci Part B Polym Phys 39:2671
14. Osuji CO, Chen JT, Mao G, Ober CK, Thomas E L (2000) Polymer 41:8897–8907
15. Mao G, Wang J, Clingman SR, Ober CK, Chen JT, Thomas EL (1997) Macromolecules 30:2556–2567
16. Fischer H, Poser S, Arnold M (1995) Liq Cryst 18:503–509
17. Anthamatten M, Hammond PT (1999) Macromolecules 32:8066–8076
18. Sänger J, Gronski W, Maas S, Stühn B, Heck B (1997) Macromolecules 30:6783–6787
19. Schneider A, Zanna J-J, Yamada M, Finkelmann H, Thomann R (2000) Macromolecules 33:649–651
20. Sänger J, Gronski W (1998) Macromol Chem Phys 199:555–561
21. Zhukov S, Geppert S, Stühn B, Staneva R, Ivanova R, Gronski W (2002) Macromolecules 35:8521–8530
22. Strobl G (1970) Acta Crystallogr A 26:367–375
23. Roe RJ (2000) Methods of X-ray and neutron scattering in polymer science. Oxford University Press
24. Mitchell GR, Windle AH (1984) Polymer 25:906–920
25. Yamada M, Iguchi T, Hirao A, Nakahama S, Watanabe J (1995) Macromolecules 28:50–58
26. Tang BZ, Kong X, Wan X, Peng H, Lam WY, Feng X-D, Kwok HS (1998) Macromolecules 31:2419–2432
27. Yamaoka K, Kaneko T, Gong JP, Osada Y (2001) Macromolecules 34:1470–1476
28. Almdal K, Rosedale JH, Bates FS, Wignall GD, Fredrickson GH (1990) Phys Rev Lett 65:1112–1115
29. Matsen MW, Bates FS (1996) Macromolecules 29:1091–1098
30. Strobl G (1996/1997) The physics of polymers. Springer, Berlin Heidelberg New York
31. Heck B, Arends P, Ganter M, Kressler J, Stühn B (1997) Macromolecules 30:4559–4566
32. Schwab M, Stühn B (1996) Phys Rev Lett 76:924–927; (1997) Colloid Polym Sci 275:341–351
33. Mittelbach P, Porod G (1961) Acta Phys Austriaca 14:405
34. Guinier A (1963) X-ray diffraction. Freeman, San Francisco
35. Schwab M, Stühn B (2000) Chem Phys 112:6461–6471
36. Wang XJ, Warner MJ (1987) Phys A Math Gen 20:713–731
37. Sänger J, Gronski W, Leist H, Wiesner U (1997) Macromolecules 30:7621–7623
38. Sänger J (1997) PhD Thesis, University of Freiburg
39. Yamada M, Itoh T, Nakagawa R, Hirao A, Nakahama S, Watanabe J (1999) Macromolecules 32:282–289
40. Zheng WY, Hammond PT (1998) Macromolecules 31:711–721
41. Terentjev EM (1995) Phys Rev E 51:1330–1337
42. Khandpur AK, Förster S, Bates FS, Hamley IW, Ryan AJ, Bras W, Almdal K, Mortensen K (1995) Macromolecules 28:8796–8806
43. Matsen MW, Bates FS (1997) J Polym Sci Part B Polym Phys 35:945–952
44. Vavasour JD, Whitmore MD (1993) Macromolecules 26:7070–7075
45. Brandrup J, Immergut EH (eds) (1989) Polymer handbook. Wiley, NY